Draft version March 23, 2016
Preprint typeset using LaTeX style emulateapj v. 03/07/07

arXiv:1603.06689v1 [astro-ph.SR] 22 Mar 2016

HST STIS OBSERVATIONS OF THE MIXING LAYER IN THE CAT'S EYE NEBULA*

Xuan Fang[1†‡], Martín A. Guerrero[1], Jesús A. Toalá[1,2], You-Hua Chu[2], and Robert A. Gruendl[3]
[1]Instituto de Astrofísica de Andalucía (IAA-CSIC), Glorieta de la Astronomía s/n, E-18008 Granada, Spain
[2]Institute of Astronomy and Astrophysics, Academia Sinica (ASIAA), Taipei 10617, Taiwan
[3]Department of Astronomy, University of Illinois, 1002 West Green Street, Urbana, IL 61801, USA
Draft version March 23, 2016

ABSTRACT

Planetary nebulae (PNe) are expected to have a $\sim 10^5$ K interface layer between the $\geq 10^6$ K inner hot bubble and the $\sim 10^4$ K optical nebular shell. The PN structure and evolution, and the X-ray emission depend critically on the efficiency of mixing of material at this interface layer. However, neither its location nor its spatial extent has ever been determined so far. Using high-spatial resolution *HST* STIS spectroscopic observations of the N V $\lambda\lambda$1239,1243 lines in the Cat's Eye Nebula (NGC 6543), we have detected this interface layer and determined its location, extent, and physical properties for the first time in a PN. We confirm that this interface layer, as revealed by the spatial distribution of the N V λ1239 line emission, is located between the hot bubble and the optical nebular shell. We estimate a thickness of 1.5×10^{16} cm and an electron density of $\sim$200 cm^{-3} for the mixing layer. With a thermal pressure of $\sim 2\times10^{-8}$ dyn cm^{-2}, the mixing layer is in pressure equilibrium with the hot bubble and ionized nebular rim of NGC 6543.

Subject headings: stars: winds, outflows — X-rays: ISM — planetary nebulae: general — planetary nebulae: individual (NGC 6543)

1. INTRODUCTION

Planetary nebulae (PNe) are formed in the final evolutionary stages of stars with initial masses $\leq$8–10 $M_\odot$. As these stars evolve along the asymptotic giant branch (AGB), they experience successive episodes of heavy mass loss through a slow (v_∞ $\sim$10 km s^{-1}) wind. Once the stellar envelope is stripped off, the hot stellar core is exposed, leading to a 1000–4000 km s^{-1} fast stellar wind (Cerruti-Sola & Perinotto 1985; Guerrero & de Marco 2013). This fast wind sweeps up the slow AGB wind, which is further photoionized by the central star (CSPN), to form a PN (Kwok 1983; Frank et al. 1990).

In this interacting stellar winds (ISW) model, an adiabatically-shocked hot bubble with temperatures as high as 10^7–10^8 K forms in the inner region of the PN, but this hot gas is too tenuous ($\sim 10^{-3}$ cm^{-3}) to be detected. Nevertheless, extended X-ray emission has now been detected inside the inner cavities of nearly 30 PNe with plasma temperatures of 1–3$\times10^6$ K and electron densities of 1–10 cm^{-3} (e.g., Kastner et al. 2000, 2012; Chu et al. 2001; Guerrero et al. 2000, 2002, 2005; Freeman et al. 2014). The detection of X-ray-emitting hot gas in PN interiors strongly supports the ISW model, but the discrepancy between the observed and predicted physical conditions and X-ray luminosities has led to the suggestion that some mechanism is reducing the temperature of the hot bubble and raising its density. Thermal conduction (Steffen et al. 2008; Soker 1994, and references therein) and/or hydrodynamical instabilities (e.g., Toalá & Arthur 2014) in the wind-wind interaction zone can inject material into the hot bubble, creating a *mixing layer* of gas with intermediate temperatures ($\sim 10^5$ K) between the hot bubble and the optical nebular shell.

As thermal conduction governs the amount of material injected into the hot bubble, turning it on or off in the models causes differences in the spatial extent and physical properties of the mixing layer. By gaining insights into the mixing layers in PNe, the effects of thermal conduction and turbulent mixing on the interior hot gas can be quantitatively assessed. This in turn helps us to refine the models to produce more realistic predictions, which can then be compared with the available sample of PNe with diffuse X-ray emission detected (Freeman et al. 2014). There is, however, very little observational information about the mixing layers.

X-ray observations of NGC 6543 (a.k.a. the Cat's Eye Nebula) reveal a physical structure qualitatively consistent with the ISW models (Chu et al. 2001). The *Chandra* image of NGC 6543 (Figure 1) shows simple limb-brightened diffuse X-ray emission confined within the bright inner shell and two blisters at the tips of its major axis, in sharp contrast to its complex optical morphology (Balick 2004), implying density enhancement near the inner nebular rim and evaporation of nebular material into hot interior. Indeed, the observed X-ray temperature (1.7×10^6 K; Chu et al. 2001) is much lower than that expected for a stellar wind of v_∞ $\sim$1400 km s^{-1} (Prinja et al. 2007). Therefore, NGC 6543 provides a case study of mixing layers in PNe.

UV lines of highly ionized species produced by thermal collisions in the mixing layer can be used as probes. The most common species are C IV, N V, and O VI, whose fractional abundances peak at $\sim1\times10^5$, 2×10^5 and 3×10^5 K, respectively (Shull & van Steenberg 1982). *FUSE* detections of the O VI $\lambda\lambda$1032,1038 doublet from

Electronic address: fangx@iaa.es

* Based on observations made with the NASA/ESA *Hubble Space Telescope*, obtained at the Space Telescope Science Institute, which is operated by the Association of Universities for Research in Astronomy, Inc., under NASA contract NAS 5-26555. The observations are associated with program #12509.

† Now at: Laboratory for Space Research, Faculty of Science, University of Hong Kong, Pokfulam Road, Hong Kong, China

‡ Also at: Department of Physics, University of Hong Kong, Pokfulam Road, Hong Kong, China

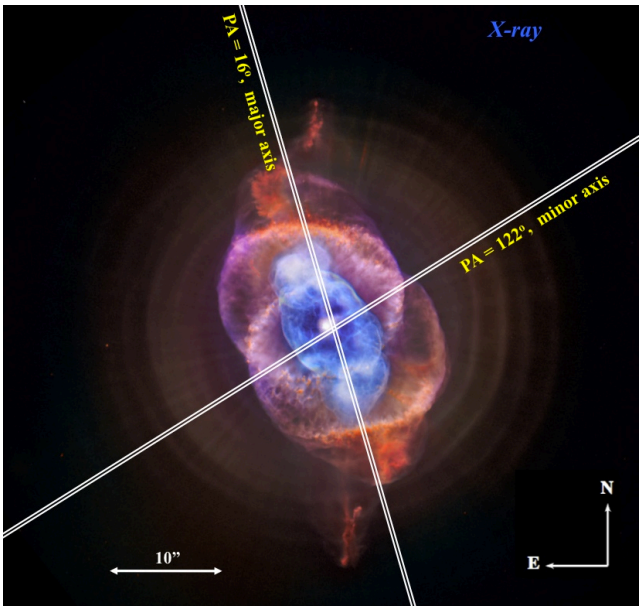

FIG. 1.— *HST* (red, purple) and *Chandra* (blue) color-composite image of NGC 6543. Image adopted from *Chandra* X-ray Center (http://chandra.harvard.edu/photo/2008/catseye/). The positions of the *HST* STIS 52″×0.″2 long slit are marked with white lines. At both PA =16° and 122°, the slit center is offset by 0.″6 from the CSPN.

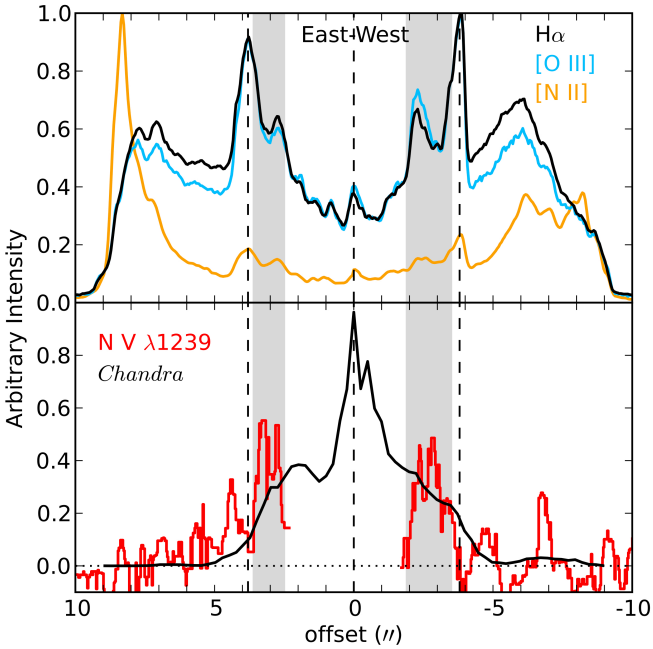

FIG. 2.— Spatial emission profiles of the Hα, [O III] λ5007, and [N II] λ6583 emission lines from the optical nebular shell (top panel), and the N V λ1239 UV resonance line from the interface layer and the *Chandra* X-ray emission from the hot bubble (bottom panel) along the minor axis of NGC 6543 at PA 122°(Figure 1). The offset is relative to the CSPN. Grey shaded areas mark the positions of the interface layer, as indicated by the N V line.

the mixing layers have been reported in several PNe (Iping et al. 2002; Ruiz et al. 2013), including NGC 6543 (Gruendl et al. 2004), but no spatial information could be drawn due to the limited angular resolution of *FUSE*. This can only be achieved by the unique capabilities of the *Hubble Space Telescope* (*HST*).

In this paper, we present *HST* STIS UV and optical spectroscopy of NGC 6543. In conjunction with the *Chandra* X-ray images, these new spectra are used to successfully determine the location and spatial extent of mixing layer in a PN for the first time. We describe the observations in Section 2, and present results and discussion in Section 3. The main conclusions are summarized in Section 4.

2. OBSERVATIONS AND DATA ANALYSIS

HST STIS UV and optical spectroscopic observations of NGC 6543 (PI: M.A. Guerrero, GO prop. ID 12509, Cycle 19) were carried out on 2012 July 3 and 2012 October 21. The observations aimed at detecting and tracing the spatial extent of the interface layer and comparing it with those of the nebular shell and hot bubble. The 52″×0.″2 long slit was placed at a position angle (PA) of 16° and 122° along the major and minor axes of the inner nebular shell (Figure 1), respectively. The G140M grating and STIS/FUV-MAMA detector were used to acquire spectra of the N V λλ1239,1243 and C IV λ1548,1551 emission lines. The observations were performed in ACCUM mode. Meanwhile, the G430L and G750M gratings and STIS/CCD detector were used to obtain information of the [O III], Hα, and [N II] lines from the optical nebular shell. The STIS/CCD observations were split into 2 exposures to allow cosmic-ray removal. A summary of the STIS configurations and exposures is given in Table 1. The spectra were reduced and calibrated with the *HST* STIS pipeline.

In order to avoid the bright stellar light, the center of the long slit was offset 0.″6 from the CSPN at each slit PA. Despite this offset, noticeable scattered stellar continuum spilt into the innermost regions of the nebular shell, reducing the detection sensitivity for the faint nebular emission within a region of radius ≃1.″5 around the CSPN.

The 2D STIS spectra were used to extract spatial profiles of emission along the minor axis of the photoionized innermost nebular shell for the Hα, [O III] λ5007, and [N II] λ6583 lines (Figure 2, top) and the collisionally-excited N V λ1239 UV line (Figure 2, bottom). The stellar light and nebular continuum were subtracted by carefully selecting spectral regions blue- and red-wards of the target emission lines. Despite this effort, the steep stellar P-Cygni profile of the N V line made it impossible to obtain a clean spatial profile of nebular emission in the innermost 3″ region around the CSPN. This inner section of spatial profile is discarded in our analysis. The spatial profile of X-ray emission, as derived from the *Chandra* observations, is added into the bottom panel of Figure 2. The spatial profiles along the major axis of the inner nebular shell of NGC 6543 (not shown here) reveal similar structures, although are complicated by projection effects of emission from the blister features.

We extracted 1D spectra from the 2D STIS UV data along the minor axis. The apertures for spectral extraction were targeted at the location of the interface layer marked by the grey shaded regions in the bottom panel of Figure 2 that have been selected according to the spatial emission profile of the N V line. The spectra extracted at the east and west positions of the interface layer were then combined and corrected for the underly-

TABLE 1
HST STIS Observing Log

Slit Position	Date	Instrumental Configuration					t_{exp}
		Detector	Grating	λ_c (Å)	Spectral Range (Å)	Dispersion (Å pixel^{-1})	(s)
NGC 6543-MINOR	2012 Jul. 3	STIS/FUV-MAMA	G140M	1222	1190–1253	0.053	4570
		STIS/FUV-MAMA	G140M	1550	1518–1581	0.053	1723
		STIS/CCD	G430L	4300	2652–5950	2.746	2×127
		STIS/CCD	G750M	6581	6248–6913	0.554	2×275
NGC 6543-MAJOR	2012 Oct. 21	STIS/FUV-MAMA	G140M	1425	1190–1253	0.053	4570
		STIS/FUV-MAMA	G140M	1550	1518–1581	0.053	1723
		STIS/CCD	G430L	4300	2652–5950	2.746	2×127
		STIS/CCD	G750M	6581	6248–6913	0.554	2×275

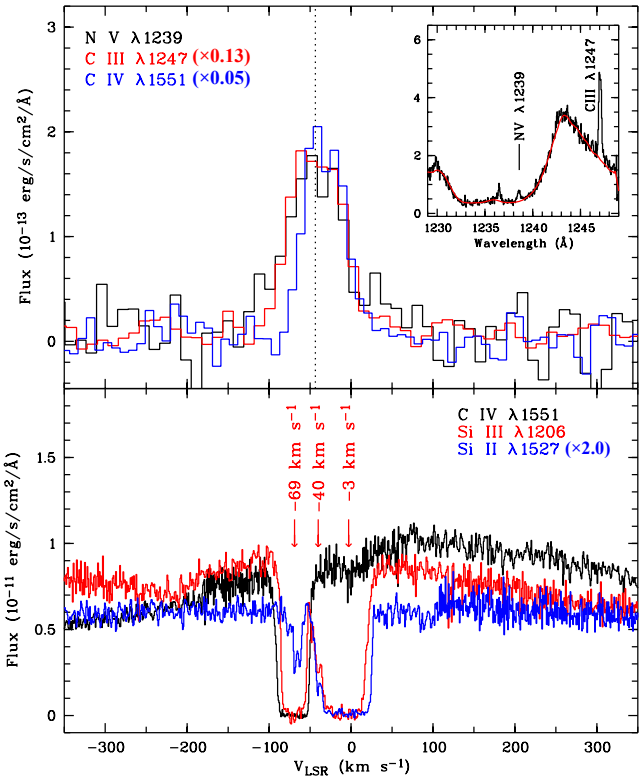

FIG. 3.— Top panel: Nebular N V λ1239, C III λ1247, and C IV λ1551 emission lines extracted at the mixing layer (Figure 2) along the minor axis of NGC 6543. Wavelengths have been converted to the LSR velocity. The radial velocity of NGC 6543 (−47.5 km s^{-1}; Miranda & Solf 1992) is marked by the vertical dotted line. Spectra are binned according to the dispersion (0.053 Å pixel^{-1}) of the STIS G140M grating. Fluxes of the C III and C IV lines are scaled by 0.13 and 0.05, respectively, to allow better comparison with the N V line. The inset shows the 1D spectrum of the mixing layer in 1229–1249 Å, and the red continuous curve is the P-Cygni profile of the CSPN. Bottom panel: STIS E140H spectrum of NGC 6543's central star corrected for the LSR velocity showing the absorption features of C IV λ1551 (black), Si III λ1206 (red) and Si II λ1527 (blue). Absorptions due to the PN shell and the interstellar gas are marked and velocities presented.

ing scattered stellar continuum. The profiles of the N V λ1239, C III λ1247, and C IV λ1551 emission lines are presented in Figure 3-top. Wavelengths have been corrected for the instrumental and orbital shifts. We then converted wavelengths to velocities by correcting for the local-standard-of-rest (LSR) velocity of the solar system (v_{LSR} = 16 km s^{-1}) towards the direction of NGC 6543 (l=96.°5, b=30.°0).

Archival *HST* STIS echelle spectra of the CSPN of NGC 6543 (PI: R.E. Williams, GO prop. ID 9736, Cycle 12) were used to complement our data analysis. The stellar spectra were obtained with the E140H grating, which provided a resolution of 114,000[4] (∼3 km s^{-1}). Three separate settings of STIS/FUV-MAMA were used to cover a wavelength region 1140–1690 Å. The 0.″2×0.″09 slit was placed on the CSPN. Detailed description of observations is given in Williams et al. (2008).

3. RESULTS AND DISCUSSION

3.1. *Emission Line Profiles*

Figure 3-top shows the N V, C III and C IV emission lines detected in our STIS G140M spectrum of NGC 6543. The N V λ1239 and C III λ1247 lines peak at the radial velocity of NGC 6543 (−47.5 km s^{-1}; Miranda & Solf 1992) and both have a full-width at half-maximum (FWHM) ∼0.33 Å. This line width is expected for an extended source filling the STIS slit width (0.″2) and actually matches that of the geocoronal Lyα emission line. This spectral resolution is insufficient to resolve the thermal width of N V λ1239 produced by the 2×10^5 K gas in the interface layer, which is estimated to have a FWHM ∼0.11 Å. Meanwhile, both lines of the C IV λλ1548,1551 doublet have a FWHM∼0.31 Å, slightly narrower than N V and C III (Figure 3, top). Moreover, its observed line center is redshifted by 0.078 Å (∼15 km s^{-1}), compared to the N V and C III lines.

Inspection of our 2D STIS spectrum reveals a narrow absorption bluewards of the C IV emission. A close look at the archival *HST* STIS E140H spectrum of NGC 6543's central star helps to clarify this issue. The spectra of the Si II λ1527, Si III λ1206, and C IV λ1551 lines have absorption features at −3, −40 and −69 km s^{-1} (Figure 3, bottom). The component at −3 km s^{-1} is saturated in Si II and Si III but weak in C IV, whereas the much weaker absorption at −40 km s^{-1} is only present in Si II and Si III. These two absorption features are generally consistent in radial velocity and relative strength with the H I 21 cm emission towards the direction of NGC 6543 detected in the Leiden/Argentine/Bonn Galactic H I Survey and Effelsberg-Bonn H I Survey (Kalberla et al. 2005; Winkel et al. 2016). Given the similar ionization potentials of H^0 and

[4] The STIS Instrument Handbook, URL http://www.stsci.edu/hst/stis/documents/handbooks

Si^+, these two absorption components can be attributed to neutral or low-excitation ionized interstellar gas along the direction of NGC 6543. On the other hand, the absorption at -69 km s^{-1} is most likely produced by the approaching side of the PN shell, as this velocity generally agrees with NGC 6543's systemic velocity ($v_{\rm LSR} = -47.5$ km s^{-1}) plus its expansion velocity ($\sim$16 km s^{-1} at the inner shell and 28 km s^{-1} at the outer shell; Miranda & Solf 1992). Furthermore, this component is weak and unsaturated in Si II, saturated in Si III, and heavily saturated in C IV, implying a higher excitation than that of the interstellar gas probed by the H I 21 cm surveys. Our identification of these absorption features generally agrees with the interpretation of *IUE* observations (Pwa et al. 1984).

The blueward absorption reduces the widths of the C IV emission lines and shifts their line centers towards the red. This explains the different emission line profiles of C IV with respect to those of N V and C III seen in Figure 3-top.

3.2. *Spatial Distribution of Line Emission*

The spatial profiles along the minor axis of NGC 6543 (Figure 2) reveal the location of mixing-layer gas originating from very different processes. The brightest emission peaks in Hα and [O III] at $\simeq$3.″9 from the CSPN mark the location of the $\sim10^4$ K swept-up inner nebular shell. The spatial profiles of the C III and C IV lines are generally consistent with those of the Hα and [O III] lines associated with the inner shell. On the other hand, the profile of the X-ray emission from the $\gtrsim10^6$ K hot gas shows an eastern peak at $\simeq$2.″0 and a shoulder of declining emission towards the west. This irregular profile is due to the low count rate, but suggests that the X-ray-emitting gas is confined within a region with radius $\leq3''$. These new profiles confirm the interpretation of Chu et al. (2001) that the X-ray-emitting gas is confined within the cool nebular shell.

Interestingly, the useful section of the spatial profile of the N V emission peaks at intermediate positions (grey shades in Figure 2), $\simeq3''$, between the optical lines from the optical nebular shell and the X-ray emission from the hot bubble. The N V ion cannot be produced by photoionization because the effective temperature of the CSPN of NGC 6543 is only $\simeq$50,000 K; thus it must be produced by thermal collisions at temperatures of $\sim10^5$ K, as expected in the mixing layer.

The observed spatial profile of the N V λ1239 emission line can be used to estimate the radius and thickness of mixing layer. Assuming a constant-emissivity cylindrical shell with radius R and thickness ΔR, we derived an outer radius of $\sim$3.″7 and a thickness 27% this radius (i.e., 1.″0). At a distance of 1.0$\pm$0.3 kpc (Reed et al. 1999), this implies a thickness of 1.5×10^{16} cm. The Hα profile can be fit similarly to derive an outer radius of 4.″6 and a thickness of 0.″9, making its inner edge coincident with the outer edge of the mixing layer.

The estimated thickness of the mixing layer in NGC 6543 can be compared with our numerical results (Toalá & Arthur 2014). Our post-AGB model with 0.633 $M_\odot$ predicts a mixing layer with a thickness of 1.8×10^{16} cm by the time the hot bubble reaches a similar average radius as that of NGC 6543 ($R_{\rm bubble} \lesssim 0.04$ pc). This is very similar to the measured thickness. However, this thickness only covers 10 cells in our current models, and thus the mixing layer is not sufficiently sampled. New high-resolution simulations are needed to make accurate predictions on the evolution and physical properties (spatial extent, density, and temperature) of the mixing layers in PNe.

3.3. *Mixing Layer Electron Density and Pressure*

We estimated the density of the mixing layer by assuming a simple geometry of the N V λ1239-emitting region: a cylindrical shell with an outer radius of 3.″7 and an inner radius of 2.″7. The intensity of the N V λ1239 line of the interface layer, as measured from the extracted spectrum, is 6.3×10^{-14} erg cm^{-2} s^{-1}. This line intensity can be expressed as:

$$I = n_{\rm e} n_{\rm N^{4+}} h\nu \frac{8.629\times10^{-6}}{\sqrt{T_{\rm e}}} \frac{\Omega(1,2;T_{\rm e})}{g_1} {\rm e}^{-\chi/kT_{\rm e}} \frac{V}{4\pi d^2}. \quad (1)$$

Here $n_{\rm e}$ and $n_{\rm N^{4+}}$ are number densities of the electron and the N^{4+} ion, respectively; $h\nu$ is the photon energy (in ergs) of the N V λ1239 line; Ω(1,2; $T_{\rm e}$) is the Maxwellian-averaged collision strength of the N^{4+} $2s\,^2S_{1/2} - 2p\,^2P^o_{3/2}$ transition, which is derived using the collision strength of N^{4+} $2s\,^2S - 2p\,^2P^o$ calculated by Cochrane & McWhirter (1983) and Equation (3.21) in Osterbrock & Ferland (2006); g_1 is the statistical weight of the lower level (for N^{4+}, $g_1 = 2$); χ is the excitation energy of the upper level (in the case of N V λ1239, $\chi = 10.008$ eV, which corresponds to 1.603×10^{-11} ergs); d is the distance to NGC 6543; V is the emitting volume in cm^3.

Here V can be derived from the STIS slit width (0.″2, corresponding to 3.0×10^{15} cm) and the cylindrical shell of the UV-emitting mixing layer (as assumed at the beginning of this section) using the equation

$$V = 2\pi\Delta x \left(\int_a^{R_1} \sqrt{R_1^2 - r^2}\ {\rm d}r - \int_a^{R_2} \sqrt{R_2^2 - r^2}\ {\rm d}r \right) \quad (2)$$

where R_1 and R_2 are the outer and inner radius of the cylindrical shell, respectively (5.5×10^{16} cm and 4.0×10^{16} cm at 1 kpc), and Δx is the thickness covered by the STIS long slit (3.0×10^{15} cm); a is the lower limit of the integration, which corresponds to 3.7×10^{16} cm from the CSPN according to the region selected for spectral extraction. The likely inhomogeneity of the 2×10^5 K, N V λ1239-emitting gas due to hydrodynamical instabilities can be accounted for by adding a filling factor, ϵ, to Equation 1.

In the interface layer, the N^{4+}/H^+ ionic abundance ratio was assumed to be close to the nebular nitrogen abundance (N/H), which is 2.30×10^{-4} (Bernard-Salas et al. 2003). This nebular abundance is consistent with the stellar wind abundance ($2.29\pm0.53\times10^{-4}$; Georgiev et al. 2008). Combining Equations 1 and 2 and by introducing a filling factor ϵ, we deduced an expression of the electron density as a function of temperature, $n_{\rm e} = 6.1\,\epsilon^{-1/2}\,T_{\rm e}^{1/4} \exp(5.808\times10^4/T_{\rm e})$. This function shows that when the temperature varies in the range 1×10^5–3×10^5 K, the electron density is always close to $\sim180\,\epsilon^{-1/2}$ cm^{-3} for the interface layer.

This density and the adopted temperature of 2×10^5 K imply a thermal pressure of $\sim2\times10^{-8}\,\epsilon^{-1/2}$ dyn cm^{-2} in

the mixing layer, which agrees with the pressure of the hot bubble and the ionized swept-up shell (Gruendl et al. 2004), probably implying the filling factor $\epsilon \sim 1$.

4. CONCLUSIONS

We present high-spatial resolution *HST* STIS UV and optical spectroscopy of the Cat's Eye Nebula (NGC 6543). Our STIS observations enabled the first view of the spatial distribution of the mixing-layer gas. This mixing layer, probed by the collisionally-ionized N V UV emission line, is located exactly between the optical nebular rim and the X-ray-emitting hot bubble as previously detected by *Chandra*.

We estimate a thickness of 1.5×10^{16} cm for the mixing layer, which is consistent with predictions of our 2D radiation-hydrodynamic simulations of the hot bubbles in PNe (Toalá & Arthur 2014). The estimated electron density and thermal pressure of this layer are found to be $\sim 180\,\epsilon^{-1/2}$ cm^{-3} and $\sim 2\times10^{-8}\,\epsilon^{-1/2}$ dyn cm^{-2}, respectively, assuming a cylindrical shell of the 2×10^5 K, UV-emitting gas. This thermal pressure agrees with that in the hot bubble and ionized nebular rim of NGC 6543, suggesting hydrodynamical equilibrium. New higher-resolution radiation-hydrodynamic numerical simulations will be carried out to investigate the evolution and properties of the mixing layer in young PNe (Toalá & Arthur, in preparation).

It is worth mentioning that the physical configuration of the mixing layer in PNe is also expected to occur within wind-blown bubbles that exhibit diffuse, soft X-ray emission such as the Orion Nebula, Wolf-Rayet bubbles, and superbubbles (e.g., Güdel et al. 2008; Jaskot et al. 2011; Ruiz et al. 2013; Toalá et al. 2012). Future UV observations towards other PNe and wind-blown bubbles, such as the Wolf-Rayet bubble NGC 6888, will help us understand and unveil the physics of the mixing layer and its relation to the existence of the diffuse X-ray-emitting gas in hot bubbles.

Support for the *Hubble Space Telescope* Cycle 20 General Observer Program 12509 was provided by NASA through grant HST-GO-12509.01-A from the Space Telescope Science Institute, which is operated by the Association of Universities for Research in Astronomy, Inc., under NASA contract NAS 5-26555. X.F., M.A.G., and J.A.T. are partially funded by grant AYA 2011-29754-C03-02 of the Spanish MEC (Ministerio de Economía y Competitividad) cofunded with FEDER funds. We thank Dr. Yong Zhang at the University of Hong Kong for discussion. We also thank the anonymous referee, whose comments help to enhance this paper. This paper utilizes the image from *Chandra* X-ray Center (http://chandra.harvard.edu/), which was operated for NASA by the Smithsonian Astrophysical Observatory and developed with funding from NASA under contract NAS8-03060. This research has made use of NASA's Astrophysics Data System (http://adsabs.harvard.edu) and the Mikulski Archive for Space Telescope (MAST, https://archive.stsci.edu/).

Facilities: HST (STIS).

REFERENCES

Balick, B. 2004, AJ, 127, 2262
Bernard-Salas, J., Pottasch, S. R., Wesselius, P. R., & Feibelman, W. A. 2003, A&A, 406, 165
Cerruti-Sola, M., & Perinotto, M. 1985, ApJ, 291, 237
Chu, Y.-H., Guerrero, M. A., Gruendl, R. A., et al. 2001, ApJ, 553, L69
Cochrane, D. M., & McWhirter, R. W. P. 1983, Phys. Scr., 28, 25
Frank, A., Balick, B., & Riley, J. 1990, AJ, 100, 1903
Freeman, M., Montez Jr., R., Kastner, J. H., et al. 2014, ApJ, 794, 99
Georgiev, L. N., Peimbert, M., Hillier, D. J., Richer, M. G., Arrieta, A., & Peimbert, A. 2008, ApJ, 681, 333
Gruendl, R. A., Chu, Y.-H., & Guerrero, M. A. 2004, ApJ, 617, L127
Güdel, M., Briggs, K. R., Montmerle, T., et al. 2008, Science, 319, 309
Guerrero, M. A., Chu, Y.-H., & Gruendl, R. A. 2000, ApJS, 129, 295
Guerrero, M. A., Chu, Y.-H., Gruendl, R. A., & Meixner, M. 2005, A&A, 430, L69
Guerrero, M. A., & de Marco, O. 2013, A&A, 553, A126
Guerrero, M. A., Gruendl, R. A., & Chu, Y.-H. 2002, A&A, 387, L1
Iping, R. C., Sonneborn, G., & Chu, Y.-H. 2002, BAAS, 34, 1254
Jaskot, A. E., Strickland, D. K., Oey, M. S., Chu, Y.-H., & García-Segura, G. 2011, ApJ, 729, 28
Kalberla, P. M. W., Burton, W. B., Hartmann, Dap, et al. 2005, A&A, 440, 775
Kastner, J. H., Montez Jr, R., Balick, B., & De Marco, O. 2008, ApJ, 672, 957
Kastner, J. H., Montez Jr, R., Balick, B., et al. 2012, AJ, 144, 58
Kastner, J. H., Soker, N., Vrtilek, S. D., & Dgani, R. 2000, ApJ, 545, L157
Kastner, J. H, Vrtilek, S. D., & Soker, N. 2001, ApJ, 550, 189
Kwok, S. 1983, in IAU Symp. 103, Planetary Nebulae, ed. D. R. Flower, p. 293
Miranda, L. F., & Solf, J. 1992, A&A, 260, 397
Osterbrock, D. E., & Ferland, G. J. 2006, Astrophysics of Gaseous Nebulae and Active Galactic Nuclei (Sausalito, CA: Univ. Science Books)
Prinja, R. K., Hodges, S. E., Massa, D. L., Fullerton, A. W., & Burnley, A. W. 2007, MNRAS, 382, 299
Pwa, T. H., Mo, J. E., & Pottasch, S. R. 1984, A&A, 139, L1
Reed, D. S., Balick, B., Hajian, A. R., et al. 1999, AJ, 118, 2430
Ruiz, N., Chu, Y.-H., Gruendl, R. A., Guerrero, M. A., Jacob, R., Schönberner, D., & Steffen, M. 2013, ApJ, 767, 35
Shull, J. M., & van Steenberg, M. 1982, ApJS, 48, 95
Soker, N. 1994, AJ, 107, 276
Steffen, M., Schönberner, D., & Warmuth, A. 2008, A&A, 489, 173
Toalá, J. A., & Arthur, S. J. 2014, MNRAS, 443, 3486
Toalá, J. A., Guerrero, M. A., Chu, Y.-H., et al. 2012, ApJ, 755, 77
Williams, R., Jenkins, E. B., Baldwin, J. A., et al. 2008, ApJ, 677, 1100
Winkel, B., Kerp, J., Flöer, L., Kalberla, P. M. W., Ben Bekhti, N., Keller, R., & Lenz, D. 2016, A&A, 585, A41